HHS Public Access

Author manuscript

Nat Neurosci. Author manuscript; available in PMC 2011 April 01.

Published in final edited form as:

Nat Neurosci. 2010 October ; 13(10): 1208–1215. doi:10.1038/nn.2634.

ADF/Cofilin-Mediated Actin Dynamics Regulate AMPA Receptor Trafficking during Synaptic Plasticity

Jiaping Gu[1], **Chi Wai Lee**[1], **Yanjie Fan**[1], **Daniel Komlos**[2], **Xin Tang**[3], **Chicheng Sun**[3], **Kuai Yu**[1], **H Criss Hartzell**[1], **Gong Chen**[3], **James R. Bamburg**[4], and **James Q. Zheng**[1]

[1]Departments of Cell Biology and Neurology, Center for Neurodegenerative Diseases, Emory University School of Medicine, Atlanta, Georgia 30322

[2]Department of Cell Biology and Neuroscience, Rutgers University, Piscataway, NJ 08854

[3]Department of Biology, Huck Institutes of Life Sciences, Pennsylvania State University, University Park, PA 16802

[4]Department of Biochemistry and Molecular Biology, Colorado State University, Fort Collins, CO 80523

Summary

Dendritic spines undergo actin-based growth and shrinkage during synaptic plasticity. The actin depolymerizing factor (ADF)/cofilin family of actin-associated proteins plays important roles in spine plasticity. Elevated ADF/cofilin activities often lead to reduced spine size and immature spine morphology, but can enhance synaptic potentiation in some cases. Therefore ADF/cofilin may exert distinct effects on postsynaptic structure and function. Here we report that ADF/cofilin-mediated actin dynamics regulate AMPA receptor (AMPAR) trafficking during synaptic potentiation, which is distinct from actin's structural role in spine morphology. We find that elevated ADF/cofilin activity markedly enhances surface addition of AMPARs after chemically-induced LTP (cLTP), whereas inhibition of ADF/cofilin abolishes AMPAR addition. Our data further show that cLTP elicits a temporal sequence of ADF/cofilin dephosphorylation and phosphorylation that underlies AMPAR trafficking and spine enlargement. These findings suggest a novel role for temporally-regulated ADF/cofilin activities in postsynaptic modifications of receptor number and spine size during synaptic plasticity.

Keywords

ADF/cofilin; postsynaptic receptor trafficking; actin dynamics; synapse

Correspondence: James Zheng, Ph.D., Department of Cell Biology, Emory University School of Medicine, 615 Michael Street, Atlanta, GA 30322. Tel: (404) 727-9133. Fax: (404) 727-6256. james.zheng@emory.edu..

Author contributions: JG, CWL, and YF contributed equally to this project: JG performed a majority of the experiments on SEP-GluR1 insertion, CWL contributed the data on actin dynamics, YF investigated cofilin phosphorylation and its contribution to spine size changes. DK performed the initial work on SEP-GluR1 imaging and cofilin regulation. XT, CS, and GC provided a majority of the electrophysiology data. KY and HCH contributed the electrophysiological recordings on neurons expressing cofilin mutants. JRB provided all cofilin reagents and insights into cofilin mechanisms and functions, and JQZ designed, planned, guided the project, as well as did some image analysis.

Introduction

Synapses of the vertebrate nervous system are highly plastic and undergo short- and long-term modifications during developmental refinement of the neural circuitry, as well as learning and memory. Synaptic modulation can occur at the pre- and post-synaptic sides of the synapse. Presynaptically, synaptic strength can be modified by altered probability of neurotransmitter release in response to each action potential. At the postsynaptic site, modification of the number, types, and properties of surface neurotransmitter receptors is believed to give rise to bidirectional plasticity of the synapse[1–4]. Several ionotropic glutamate receptors are involved in excitatory synaptic transmission, of which alpha-amino-3-hydroxy-5-methyl-4-isoxazolepropionic acid receptors (AMPARs) are best known for their rapid trafficking into and out of the synapse by cycling between intracellular stores and the cell surface during synaptic potentiation and depression, respectively[1–4]. Most of the excitatory synapses in the vertebrate brain reside on dendritic spines, tiny actin-based membrane protrusions that serve as the platform for postsynaptic specializations. Growth and shrinkage of dendritic spines have also been associated with long term potentiation and depression (LTP and LTD), respectively[5–7]. It is generally thought that the morphological changes of postsynaptic spines are coupled to receptor trafficking during plasticity, which may function to dynamically adjust the membrane area for accommodating the changing number of synaptic receptors[8–10].

The actin cytoskeleton plays an important role in postsynaptic structure, function, and plasticity[10–12]. Actin is highly enriched in spines and provides the structural foundation for distinct spine shape, size, and changes associated with synaptic modification. Additionally, the actin cytoskeleton supports the scaffold for postsynaptic specializations that include the localization and clustering of glutamate receptors for efficient synaptic transmission. Actin depolymerizing factor (ADF) and cofilin regulate the dynamics of the actin cytoskeleton through their filament-severing and monomer-binding activities[13, 14]. The activity of ADF/cofilin is largely regulated through phosphorylation of its serine-3 (Ser3) residue by LIM kinases (LIMKs) for inactivation and dephosphorylation by Slingshot (SSH) or chronophin phosphatases for activation, although alternative mechanisms do exist[14]. ADF/cofilin phosphorylation and dephosphorylation have been associated with spine growth and shrinkage during LTP and LTD, respectively[15–17]. Lack of LIMK-1 resulted in elevated ADF/cofilin activity that leads to immature spines with reduced size and filopodia-like shape, but surprisingly enhanced LTP[18]. It is thus conceivable that ADF/cofilin may regulate synaptic strength by mechanisms distinct from those that control spine morphology. In this study, we present evidence that ADF/cofilin-mediated actin dynamics play an important role in postsynaptic trafficking and membrane addition of AMPA receptors during synaptic plasticity. Using live imaging to directly examine surface addition of AMPARs in single spines, we first show that elevated ADF/cofilin-mediated actin dynamics are essential for AMPAR addition during chemically-induced LTP (cLTP). We further provide evidence that rapid addition of AMPARs during cLTP is not directly coupled to a change in spine size. Instead, surface AMPAR addition and spine enlargement appear to be temporally separated and depend on ADF/cofilin activation and inactivation, respectively. These findings thus point to an exciting mechanism by which temporally regulated ADF/cofilin-

mediated actin dynamics regulate postsynaptic receptor trafficking and structural modifications for synaptic potentiation.

Results

Rapid trafficking of AMPARs to spine surface during cLTP

To investigate rapid AMPAR trafficking at dendritic spines, we expressed super-ecliptic pHluorin fused to the N-terminus of glutamate receptor 1 (SEP-GluR1) in cultured hippocampal neurons and used live confocal imaging to examine the dynamic changes in SEP-GluR1 fluorescence. Since the fluorescence of SEP is quenched when SEP-GluR1 is in the acidic environment of vesicular compartments, this imaging approach enables us to detect the surface presence of SEP-GluR1 due to its strong fluorescence at pH 7 and above[19, 20]. To include spines in different focal planes, we performed a complete confocal z-sectioning of the dendritic region of interest, followed by maximal intensity projection to produce a 2-D image (see Methods). We found that SEP-GluR1-expressing neurons of 21 days in vitro (DIV21) exhibited numerous spines along the dendritic processes, of which many were highlighted by strong SEP-GluR1 fluorescence (Fig. 1a). The strong SEP-GluR1 fluorescence at spines is consistent with the notion that spines are the platform for postsynaptic specializations with concentrated glutamate receptors. On the other hand, the dendritic shaft, as well as some of the spines, displayed a much lower level of SEP-GluR1 fluorescence, indicating a minimal level of diffusely distributed SEP-GluR1. It is plausible that the spines lacking significant SEP-GluR1 fluorescence might represent the postsynaptic terminals of silent or inactive synapses[21].

To study changes in surface AMPARs during synaptic plasticity, we adopted a method to chemically induce LTP (cLTP) by a brief exposure of cells to a potassium channel blocker tetraethylammonium (TEA)[22]. Electrophysiological recordings of miniature excitatory postsynaptic currents (mEPSCs) showed that this TEA-cLTP method could effectively potentiate synaptic transmission over an extended period of time (~ 2 hr) in our high-density hippocampal cultures (Fig. 2). Specifically, 10 min exposure to 25 mM TEA resulted in a marked increase in the mEPSC frequency that lasted over 2 hr (Fig. 2b). The median amplitude of mEPSCs followed a similar potentiation trend after TEA treatment but without statistical significance (Fig. 2c), which may be attributed to the presence of mEPSCs without amplitude changes. Indeed, the cumulative distribution plot of mEPSC amplitudes revealed that TEA stimulation elicited a significant amplitude increase in a population of the mEPSCs in the first 20 min (Fig. 2d, $p<0.0001$, Kolmogorov-Smirnov test). The amplitude increase became much smaller for mEPSCs recorded 20–40 min after TEA treatment. When all mEPSCs after TEA-cLTP stimulation (>2 hr period) were averaged, no difference in the amplitude was seen (Fig. 2f). Consistent with previous findings[22], TEA-cLTP is AMPAR-dependent, as CNQX, an AMPAR antagonist but not AP5, a NMDAR blocker, was able to block the potentiation (Fig. 2e). In support of the electrophysiological data, we found that 10 min TEA stimulation resulted in a marked increase in SEP-GluR1 fluorescence in many dendritic spines (Fig. 1a, magnified views in the right panels, arrows). We measured the integrated intensity of SEP-GluR1 fluorescence of each spine before and after TEA-cLTP and calculated the relative change ($\Delta F/F$). We found that, on average, TEA-cLTP resulted in

~20% increase in spine SEP-GluR1 fluorescence per cell (Fig. 1a, b). 10 min exposure to Hepes-buffered saline (HBS) alone did not produce any effects on SEP-GluR1 fluorescence (Fig.1b). We confirmed that SEP-GluR1 fluorescence reflects SEP-GluR1 on the cell surface by exposing the cells to a membrane impermeable acidic buffer of pH 6.0[23], which resulted in a marked and immediate loss of SEP fluorescence (Fig. 1a). The SEP-GluR1 fluorescence was found to fully recover shortly after returning the cells to pH 7.4. Therefore, TEA-induced cLTP results in robust addition of new AMPARs to the postsynaptic surface.

The TEA-induced increase in spine SEP-GluR1 fluorescence is further supported by the cumulative ΔF/F distributions of all spines examined (Fig. 1c). TEA elicited a marked increase in the number of spines with positive ΔF/F values and shifted the distribution to the right. Since only a portion of spines responded to TEA with an increase in SEP-GluR1 fluorescence, we used an intensity threshold to select the spines with SEP-GluR1 fluorescence brighter than that of the dendritic shaft (see Supplemental fig. 1) and determined the numbers of spines exhibiting bright SEP-GluR1 fluorescence before and after TEA-cLTP. While this quantification method is likely to miss small changes in SEP-GluR1 fluorescence of some spines, it enables us to determine the number of spines exhibiting a definite increase in SEP-GluR1 fluorescence. We found that 10 min exposure to TEA, not HBS, resulted in a ~30% increase in the number of spines exhibiting bright SEP-GluR1 fluorescence (Fig. 1b). The increase in SEP-GluR1 signals after TEA treatment was blocked by 10 μM CNQX, but not by 100 μM AP5 (Fig. 1b, c), supporting the conclusion that TEA-cLTP is AMPAR-dependent. Moreover, fast time-lapse imaging revealed that SEP-GluR1 addition to spine surface was rapid and mostly occurred within a few minutes (<5 min) upon TEA application (Supplemental Fig. 2). Finally, to ensure that the results were not due to an artifact of exogenous expression of SEP-GluR1, untransfected hippocampal neurons were treated for cLTP as described above but subsequently fixed and immunostained for surface GluR1. Consistently, we observed an increase in the surface GluR1 immunofluorescence similar to that observed in the SEP-GluR1 imaging (Supplemental Fig. 3), indicating that endogenous GluR1 goes to the surface membrane upon TEA-cLTP.

Actin dynamics are required for AMPAR trafficking

We tested if the actin cytoskeleton plays a role in the trafficking of AMPARs during synaptic plasticity. We first employed Latrunculin A (Lat A), an agent known to inhibit actin polymerization by sequestering actin monomers, to investigate if the inhibition of actin polymerization (without disrupting the existing actin network) could affect the surface addition of AMPARs during cLTP. We pretreated the DIV21 hippocampal neurons expressing SEP-GluR1 with varying Lat A concentrations for 20 min, followed by 10 min cLTP induction. Live confocal imaging of SEP-GluR1 was performed at the beginning of Lat A treatment, and before and after cLTP induction. We used the images at the onset of Lat A treatment and the beginning of cLTP treatment to determine the effect of Lat A on the baseline of SEP-GluR1 enrichment at the spines. The images at the onset and 10 min after cLTP were used to determine SEP-GluR1 insertion after cLTP. We first established that SEP-GluR1 signals at spines did not change in a 20 min control period without any drug application or during 10 min exposure to HBS, but markedly increased after TEA-cLTP

induction (Fig. 3). Lat A was found to exert profound dose-dependent effects on SEP-GluR1 signals at spines and insertion during TEA-cLTP. At a high concentration (2 μM), 20 min of Lat A treatment caused a marked decline in SEP-GluR1 fluorescence at spines, which continued during 10 min cLTP treatment. Some spines also shrunk upon 2 μM Lat A treatment (Fig. 3a, arrowheads). Therefore, we suspect that 2 μM Lat A adversely affected the integrity of the actin network required for spine receptor anchoring and clustering[24].

When Lat A was used at 200 nM, no obvious alteration in spine morphology was observed (Fig.3a), which was confirmed by phalloidin staining (Supplemental fig. 4). However, SEP-GluR1 fluorescence intensity on spines was reduced by about 10%, indicating that this concentration of Lat A minimally affected the baseline AMPARs. Importantly, 200 nM Lat A abolished the surface addition of SEP-GluR1 after cLTP stimulation (Fig. 3b). At 20 nM, Lat A was found to block the increase of SEP-GluR1 induced by TEA-cLTP without affecting either spine morphology or the baseline SEP-GluR1 on spines after 20 min pretreatment (Fig. 3b). Furthermore, the basal synaptic transmission was not affected by 20 nM Lat A (Supplemental fig. 5). Therefore, AMPAR insertion during cLTP is dependent on actin polymerization.

To further elucidate the role of actin dynamics in AMPAR trafficking during synaptic plasticity, we utilized another membrane-permeable actin-binding drug, Jasplakinolide. Jasplakinolide is a natural cyclic peptide that binds actin filaments at the same site as phalloidin to promote actin polymerization and stabilize the actin filaments by inhibiting depolymerization[25]. We tested different concentrations of Jasplakinolide on SEP-GluR1 localization and insertion in spines. Unlike Lat A, Jasplakinolide did not affect the baseline SEP-GluR1 levels after 20 min pre-treatment. However, we found that Jasplakinolide at 1 μM, but not 100 nM, largely blocked the insertion of SEP-GluR1 in response to cLTP stimulation (Fig. 3). We also confirmed that 1μM Jasplakinolide did not affect dendritic actin networks and spine morphology, as well as baseline synaptic transmission (Supplemental Fig. 4 and 5). Since Jasplakinolide functions to stabilize the actin filaments and inhibit depolymerization, these results suggest that actin depolymerization is also required for receptor insertion. Together with the results involving Lat A blockade of SEP-GluR1 insertion, we conclude that while a stable actin network is required for AMPAR clustering and anchoring at the spine, bi-directional dynamics of the actin cytoskeleton (assembly and disassembly) are required for the rapid addition of AMPARs to spine surface during cLTP.

ADF/cofilin regulates AMPAR addition to spine surface

ADF/cofilin represents an important family of proteins that profoundly regulate actin dynamics. We therefore tested if ADF/cofilin is involved in AMPAR insertion during cLTP. We first used the peptidomimetic approach to alter the endogenous ADF/cofilin activity and examined AMPAR trafficking during cLTP. Here, peptides containing a 16 amino acid sequence of the cofilin Ser3 or phospho-Ser3 site (referred to as S3 or pS3 peptides) were used to inhibit LIMKs or SSH, respectively. These peptides also contain a 16 amino acid sequence of penetratin for cell internalization and have been widely used to effectively alter the endogenous ADF/cofilin activity in cells[16, 26, 27]. We applied the particular peptide to

cultured hippocampal neurons expressing SEP-GluR1 6 hr prior to cLTP induction. This 6 hr pre-treatment time was previously established for effective internalization and alteration of cofilin activity[27]. We found that S3 peptides markedly enhanced, whereas pS3 peptides inhibited, SEP-GluR1 trafficking to spine surface during TEA-cLTP (Fig. 4a). Quantitative analysis shows that S3-treated neurons exhibited a greater increase in both the number of spines with bright SEP-GluR1 fluorescence (Fig. 4b) and the ΔF/F of spine SEP-GluR1 signals (Fig. 4c) in response to TEA-cLTP than non S3-treated neurons. Neurons treated with pS3 peptides, however, were impaired in AMPAR insertion induced by TEA-cLTP. The reverse S3 peptides (the same 16 residues as the S3 peptide, but in reverse order and with a normal penetratin sequence) had no effect on SEP-GluR1 insertion after cLTP. These data suggest that the ADF/cofilin activity is required for AMPAR insertion during cLTP.

We also analyzed baseline AMPAR presence on dendritic spine surface before and after 6 hr S3 or pS3 peptide treatment. We found that S3 peptide reduced the baseline number of spines and SEP-GluR1 puncta by ~10%, whereas pS3 peptide did not exert any significant effects (Fig. 4d). While the reduction in SEP-GluR1 level with 6 hr S3 peptide treatment is relatively small, it suggests that a prolonged increase in ADF/cofilin activity may negatively impact surface AMPAR level at the spine. The apparently opposite effects of ADF/cofilin on baseline AMPARs and LTP-induced surface addition suggest that ADF/cofilin may play different roles in AMPAR insertion and surface clustering. The finding that the spine head/neck ratio (based on analysis on co-expressed mOrange signals) was not significantly changed by either peptide (Fig. 4e) suggests that the effects of ADF/cofilin on AMPAR trafficking did not result from their action on the spine structure.

The dependence of AMPAR insertion during cLTP on ADF/cofilin activation was further supported by molecular manipulations using various forms of cofilin 1 (WT: wild-type; S3A: constitutively active in which Ser3 is mutated to alanine; S3E: dominant negative in which Ser3 is mutated to glutamic acid). We found that expression of WT cofilin 1 did not alter the insertion of AMPAR after 10 min cLTP (Fig. 5a). Both the control and WT groups of neurons exhibit similar increases in the ΔF/F of SEP-GluR1 fluorescence (Fig. 5b). Importantly, the increased SEP-GluR1 signals were sustained over 1 hour after the 10 min cLTP induction by TEA, which is consistent with the electrophysiological data on lasting cLTP by TEA. In support of the peptidomimetic results, S3A markedly enhanced, whereas S3E abolished, the insertion of SEP-GluR1 to spine surface induced by TEA-cLTP (Fig. 5a, b). The effects of S3A and S3E on TEA-cLTP were also supported by electrophysiological recordings (Supplemental fig. 6). Since cofilin and its mutants were expressed in hippocampal neurons for 7 days before the cLTP induction and imaging, we therefore examined if overexpression of these exogenous molecules exerted any effects on the spine development and baseline AMPAR presence on the spines. We found that the baseline level of spine density, as well as the number of spines exhibiting bright SEP-GluR1 fluorescence, was not significantly different among the WT, S3A, and S3E groups (Fig. 5c). Given that these mutant proteins were expressed on top of endogenous ADF/cofilin, the development of spines and synapses might have been maintained by the endogenous ADF/cofilin molecules. Nonetheless, we conclude that ADF/cofilin activity is required for surface addition of AMPARs during synaptic potentiation.

Temporal regulation of AMPAR addition and spine size by ADF/cofilin

Our time-lapse imaging found that surface addition of SEP-GluR1 did not involve obvious spine enlargement (Supplemental fig. 2), suggesting that these two events may not be necessarily coupled. To further address this question, we analyzed the correlation between AMPAR insertion (visualized by SEP-GluR1) and the morphological change of the same spine (visualized by mOrange) during TEA-cLTP. We found that about 50% of spines that exhibited substantial SEP-GluR1 insertion after 10 min TEA stimulation were not accompanied by a change in their size (Fig. 6a). About 30% and 15% of spines with significant SEP-GluR1 insertion were found to be enlarged and newly formed, respectively. For spines that did not show a significant increase in SEP-GluR1 insertion (either those with weak SEP-GluR1 or strong SEP-GluR1 fluorescence), a majority of them (~80%) did not exhibit any changes in size after the 10 min cLTP treatment (Fig. 6a). The scatter plot of the ΔF/F of spine SEP-GluR1 vs. the change in spine size of all the spines examined showed a very weak correlation (Fig. 6b, r^2=0.19). These results suggest that AMPAR insertion during cLTP is not coupled to spine enlargement or new spine formation.

We further investigated the change in spine size during and after TEA-cLTP and found that spine enlargement and new spine formation mostly occurred 20 min after the completion of 10 min TEA-cLTP induction (Fig. 7a). Quantification showed that the average increase in spine size (from several hundreds of spines) reached over 30% at 20 min after the 10 min TEA-cLTP stimulation, compared to only ~10% at the end of 10 min TEA treatment (Fig. 7b). We next tested the dependence of spine size increase on ADF/cofilin activity by expressing RFP-cofilin S3A or S3E together with GFP for assessing the spine size. Interestingly, S3A, but not S3E, abolished the spine enlargement during and after TEA-cLTP induction. These results support the notion that inactivation of cofilin is required for spine enlargement after LTP[15, 17], but are opposite to our finding that ADF/cofilin activation is required for AMPAR insertion during cLTP. Considering the temporal segregation of AMPAR insertion and spine enlargement and their differential dependence on ADF/cofilin activities, we speculated that a temporal sequence of ADF/cofilin-mediated actin dynamics may regulate and coordinate the two important events leading to synaptic potentiation.

To test this temporal model, we examined the phosphorylation of cofilin using an antibody raised specifically against phosphorylated cofilin (p-cofilin). We found that the p-cofilin level in DIV21 hippocampal neurons exhibited a marked decline at 2 or 5 min after the onset of TEA treatment, but significantly increased by 30 min after TEA washout (Recovery). The total cofilin (t-cofilin) level, as detected by a pan cofilin antibody, did not show significant changes before, during, and after TEA application (Fig. 8a; for the original blot, please see Supplemental fig. 7). To better depict the changes in cofilin phosphorylation, we quantified the western data and normalized the p-cofilin signal against the t-cofilin level. We found that cLTP induction by TEA caused a transient decrease of the p/t-cofilin ratio, indicating a transient cofilin dephosphorylation and activation (Fig. 8a). When those neurons recovered for 30 min after 10 min TEA treatment, the p/t-cofilin ratio increased toward the control level (Fig. 8a). A major function of activated ADF/cofilin molecules is to sever existing actin filaments for increased actin dynamics, which generates new barbed ends of actin

filaments. We therefore labeled the barbed ends of actin filaments in cultured hippocampal neurons before, during, and after the 10 min TEA treatment. We found that in untreated cells actin barbed ends were present throughout the dendritic processes with some localizing to dendritic spines (Fig. 8b). When the neurons were exposed to TEA for cLTP induction, a marked increase in actin barbed ends was observed (Fig. 8b). Quantitative analyses show that the number of actin barbed ends was almost doubled by TEA treatment when compared to the control. More importantly, the percentage of spines containing actin barbed ends increased about two folds after TEA exposure (Fig. 8b). The level of actin barbed ends returned to normal 30 min after TEA washout, which is consistent with the p/t-cofilin pattern. Together, these data support the notion that ADF/cofilin becomes transiently activated by dephosphorylation during the 10 min TEA-cLTP induction. The temporal sequence of ADF/cofilin dephosphorylation and phosphorylation coincides with AMPAR insertion and spine enlargement, respectively, and may underlie the changes in postsynaptic receptor trafficking and structure leading to synaptic potentiation.

Discussion

The actin cytoskeleton is well known for its structural role in dendritic spine development and plasticity[11], [12]. In this study, we have uncovered a novel role for the actin cytoskeleton in synaptic receptor trafficking during plasticity. Our data show that ADF/cofilin-mediated actin dynamics regulate AMPAR trafficking to the postsynaptic surface during cLTP. Using live imaging, we first show that while the integrity of the actin cytoskeleton is essential for the receptor clustering on the postsynaptic surface, actin dynamics are required for AMPAR insertion during cLTP. Second, we find that ADF/cofilin-mediated actin dynamics regulate AMPAR trafficking during synaptic potentiation: elevated ADF/cofilin activities potentiate whereas ADF/cofilin inhibition abolishes AMPAR insertion. Third, we show that rapid AMPAR insertion during cLTP is not directly coupled to the morphological changes of dendritic spines. Instead, spine enlargement elicited by cLTP lagged temporally behind the AMPAR insertion. Finally, we have uncovered an intriguing temporal sequence of ADF/cofilin dephosphorylation and phosphorylation that underlie AMPAR insertion and spine enlargement, respectively. It is thus conceivable that a transient activation of ADF/cofilin by dephosphorylation during cLTP generates the actin dynamics required for AMPAR insertion and the subsequent inactivation via phosphorylation enables actin polymerization for spine growth and receptor anchoring and clustering.

The actin cortex in many cells is known to present a physical barrier for vesicle fusion with the plasma membrane[28], [29]. Therefore, dynamic remodeling of the cortical actin by ADF/cofilin may be required for vesicular delivery of AMPARs to the surface. However, studies from non-neuronal cells have established that actin actively participates in vesicular trafficking to and from the plasma membrane[30]. While our data can not definitely address the precise role for ADF/cofilin-mediated actin dynamics in AMPAR trafficking during LTP, the effective blockage of AMPAR insertion during cLTP by Lat A appears to rule out a simply passive role for the actin dynamics. Lat A binds to actin monomers to prevent filament assembly and can lead to the disruption of the existing actin cytoskeleton at high concentrations[31]. The finding that Lat A at 20 nM or higher concentrations abolished the insertion of AMPARs (Fig. 3) suggests that actin assembly is required for AMPAR insertion

during cLTP. The fact that stabilization of actin filaments by Jasplakinolide also blocked AMPAR insertion suggests that actin disassembly might also be required. The Jasplakinolide data are consistent with previous studies in which phalloidin, which stabilizes actin filaments, attenuated the LTP magnitude[32]. While the ADF/cofilin severing activity can break down the existing actin filaments, it can also generate new barbed ends for further actin polymerization. It is thus conceivable that ADF/cofilin-mediated actin dynamics may produce two coordinated effects on the actin network for AMPAR insertion: temporary removal of the actin cortical barrier followed by promotion of new actin assembly for the vesicular delivery of AMPAR to the surface (Supplemental fig. 8). While our preliminary test involving paGFP-actin suggests an increase in actin turnover in spines during TEA-cLTP (Supplemental fig.9), the validation of this hypothesis and elucidation of the actin mechanisms controlling AMPAR trafficking require future experiments that employ high-resolution imaging of the spatiotemporally restricted actin remodeling and vesicle fusion simultaneously.

The spatial organization and dynamics of the actin cytoskeleton in dendritic spines have just begun to be elucidated[12]. ADF/cofilin is present in dendritic spines and its knockdown affects the actin turnover and morphology of the spines[33]. Interestingly, siRNA knockdown of cofilin 1 appears to reduce the mEPSC frequency[33], suggesting a potential function for ADF/cofilin in synaptic transmission. Given that cofilin molecules were found to concentrate in the spine periphery, close to the plasma membrane[34], ADF/cofilin-mediated actin dynamics could regulate membrane recycling of AMPARs outside of the PSD region. It should be noted that surface addition of AMPARs does not necessarily need to be confined in spines, but can occur in extrasynaptic dendritic regions followed by lateral movement into spines[35], [36]. ADF/cofilin-mediated actin dynamics could potentially affect the lateral diffusion of surface AMPARs to contribute to synaptic plasticity as well[37]. Finally, recent studies suggest that phosphorylated cofilin may stimulate Phospholipase D1 (PLD1)[38], which could potentially affect vesicular trafficking of AMPARs through its influence on the membrane. However, our experiments involving actin drugs LatA and Jasp support the notion that inhibition of actin dynamics negatively impact AMPAR insertion during cLTP.

Our analyses of AMPAR insertion and spine size indicate that these two events are not directly coupled, which is consistent with an emerging view on the decoupling between spine size and synaptic strength[11]. Additional support on the decoupling came from studies involving ADF/cofilin. Increased ADF/cofilin activity is often associated with a reduction in spine size[16], [18] but could enhance synaptic potentiation in some cases[18]. On the other hand, a large body of literature has documented spine enlargement and actin polymerization after LTP induction[8], [39], [40]. Inhibition of cofilin activity by phosphorylation was also observed to accompany spine enlargement during LTP[15], [17], but SSH knockdown (presumably leading to enhanced ADF/cofilin phosphorylation) impaired AMAPR-dependent synaptic potentiation[41]. The apparent contradictions among these results might be explained by a temporal sequence of ADF/cofilin dephosphorylation and phosphorylation underlying postsynaptic changes in AMPARs and spine size, respectively. Indeed, we found that ADF/cofilin exhibited a transient dephosphorylation (activation) during TEA-cLTP induction and then recovered to the pre-stimulation phosphorylation level, which coincide with that of

AMPAR insertion and spine enlargement. Given that TEA-induced cLTP involves Ca^{2+} signaling and calcineurin activation[42], a temporal pattern of Ca^{2+} signals might be responsible for the brief ADF/cofilin dephosphorylation followed by phosphorylation. Importantly, we found that constitutively active cofilin (S3A) enhanced AMPAR insertion but abolished spine enlargement whereas the dominant negative cofilin (S3E) blocked AMPAR insertion without affecting spine enlargement. Therefore, these findings suggest that spatiotemporal regulation of the actin structure and dynamics may support and regulate a sequence of postsynaptic events leading to synaptic potentiation: receptor insertion at extrasynaptic sites, stabilization of the actin network for synaptic capture, anchoring and immobilization of receptors, and spine enlargement through actin polymerization to accommodate the increasing number of receptors on the surface (Supplemental fig. 8). Our findings are consistent with an increasing number of studies on the active role for actin-based mechanisms for synaptic receptor trafficking[43–45]. Given that the ADF/cofilin regulation is altered in a number of neurological disorders, including Williams Syndrome[46], these findings could also shed light on the molecular and cellular mechanisms underlying some of the synaptic defects associated with the disorders.

Methods

Constructs and reagents

DNA constructs of pmOrange and pEGFP-N1 were from Clontech. The mOrange coding sequence was subcloned into pEGFP-N1 vector (with green fluorescent protein sequence excised) to allow expression in mammalian cells. pCi-SEP-GluR1 construct was a gift from Dr. Roberto Malinow at University of California at San Diego. Human cofilin wt, S3A and S3E cDNAs with the stop codon removed by PCR modification were cloned into the pmRFP vector[47] as previously described[48]. The S3, pS3 and rev-S3 peptides were synthesized by GenScript (Piscataway, NJ), which contain 16 amino acids of the N-terminal sequence of cofilin (MASGVAVSDGVIKVFN), or in phosphorylated form (MAS(p)GVAVSDBVIKVFN), or in reverse order (NFVKIVGDSVAVGSAM), together with a penetratin sequence (RQIKIWFQNRRMKWKK). All the peptides were used at 20 μg/ml. Fluorescent secondary antibodies and Jasplakinolide were from Invitrogen. Latrunculin A was from Sigma.

Hippocampal neuron culture and transfection

Sprague Dawley timed pregnant rats were purchased from Charles River Laboratories (Wilmington, MA). Primary hippocampal neurons were prepared from E18 rat embryos and plated on 25mm coverslips or 35mm glass bottom dishes pretreated with 0.1 mg/mL poly-D-lysine, at a density of approximately 350,000 cells per dish. Neurons were plated and maintained in Neurobasal medium supplemented with B-27 and GlutaMax (Invitrogen). Cells were transfected with Calphos calcium phosphate transfection kit (Clontech) at DIV 14–16 and imaged between DIV 21–23. All the experiments were carried out in accordance to the NIH guideline for animal use and have been approved by the Institutional Animal Care and Use Committee (IACUC) of Emory University.

Live-cell imaging and cLTP treatment

Neurons were changed from culture medium to a HEPES buffered recording solution (140 mM NaCl, 5 mM KCl, 2 mM $CaCl_2$, 1.5 mM $MgCl_2$, 10 mM glucose, 25 mM HEPES, pH 7.4). Coverslips with neurons were mounted onto a heating chamber and maintained at 37°C during imaging. Chemical LTP medium was a modified recording solution with high calcium (5 mM) and low magnesium (0.1 mM), containing 25 mM TEA (Sigma). After the first image was taken, recording solution was replaced with the cLTP medium for 10 min, before being changed back to recording solution. To include spines in different focal planes, a complete confocal z-sectioning of the dendritic region of interest (~12 slices) was acquired, followed by maximal intensity projection to produce a 2-D image. A Nikon C1 laser scanning confocal system on a Nikon inverted microscope was used for most of the imaging experiments.

Electrophysiology

Whole-cell patch clamp recordings were performed using Multiclamp 700A amplifier (Axon Instruments) as described before[49]. Patch pipettes were pulled from borosilicate glass and fire-polished (4–6 MΩ). The recording chamber was continuously perfused with HEPES buffered recording solution and switched to chemical LTP stimulation medium for 10 min, the same protocol used for imaging studies. The pipette solution contained 125 mM K-Gluconate, 10 mM KCl, 5 mM Tris-phosphocreatine, 5 mM EGTA, 10 mM HEPES, 4 mM MgATP, 0.5 mM Na_2GTP, pH 7.3 adjusted with KOH. The membrane potential was clamped at −70 mV. Data were acquired using pClamp 9 software, sampled at 5 kHz and filtered at 1 kHz. For mEPSC recordings, 0.5 μM TTX and 20 μM bicuculline (or 100 μM picrotoxin) were added to block action potentials and $GABA_A$ receptors. Off-line data analysis of mEPSCs was performed using MiniAnalysis software (Synaptosoft). Data were expressed as mean value ± standard errors and unpaired Student's t test was used for statistical analysis, unless otherwise stated.

Quantitative analysis

3-D image stacks were taken on dendritic regions of a neuron and then projected to 2-D images using maximal intensity. To count the numbers of spines with bright SEP-GluR1 fluorescence, the same threshold was set for both images (before and after cLTP) in the green channel to highlight postsynaptic receptor clusters. Then the number of receptor clusters was automatically counted using ImageJ. The integrated intensity of SEP-GluR1 signal on every spine was also measured in both images to calculate spine $\Delta F/F_0$. Sum of SEP-GluR1 signals of all spines in one neuron before and after cLTP was used to calculate $\Delta F/F_0$ for the entire neuron. For spine size analysis, we measured the integrated intensity of mOrange or GFP signals in the entire spine before and after TEA treatment to detect volume changes of the spine. In Fig. 6, panel a, we consider any spines showing more than 30% increase of integrated intensity as enlarged spines, and those with more than 30% decrease as shrunken spines. Spines with changes in integrated intensity under 30% were categorized as no change in size.

Immunostaining

For surface GluR1 staining, neurons were incubated with antibody against the N-terminus of GluR1 (Calbiochem) in recording solution for 20 min at 37 °C, washed with PBS and fixed with 4% paraformaldehyde (PFA) and 4% sucrose in PBS for 20 min and incubated with appropriate secondary antibody in 1% BSA for 45 min before imaging. For F-actin labeling, neurons were first fixed for 20 min in 4% PFA before permeabilizing with 0.1% Triton in PBS 10 min and labeling with Alexa 488-phalloidin for 15 min (Invitrogen, 1:1000).

Western blot

DIV21 cultures of hippocampal neurons were gently washed with the recording solution and then exposed to the cLTP solution containing TEA or the recording solution for the specific durations indicated. For the group of recovery, the cultures were washed twice with the recording solution after TEA treatment and incubated at 37°C for additional 15 min or 30 min. After treatment, cells were washed quickly with the recording solution and extracted with lysis buffer on ice (RIPA Lysis buffer supplemented with protease inhibitor cocktail (Santa Cruz, SC-24948) and phosphatase inhibitors (Sigma, P2850)). Extracts were dissolved in NuPage sample buffer (Invitrogen) with 50mM DTT and heated at 85 °C for 5min. Equal amount of protein was loaded and fractioned by SDS-PAGE in a 12% acrylamide gel and subsequently transferred to nitrocellulose membrane. Membranes were treated with 5% milk in PBS buffer with 0.05% Tween-20 and then blotted with primary antibody: anti-cofilin (Abcam, ab42824, 1:1000), anti-phospho-cofilin (Abcam, ab12866, 1:1500). Bounded antibodies were detected by HRP conjugated secondary antibody (Jackson ImmunoResearch), visualized by chemiluminescence using ECL (Pierce), and quantified using the gel analysis routine of ImageJ software (NIH).

Visualization of actin barbed ends

Free F-actin barbed ends were labeled with 0.45 μM rhodamine-conjugated G-actin (Cytoskeleton) for 2 min in the saponin permeabilization solution (20 mM HEPES, 138 mM KCl, 4 mM $MgCl_2$, 3 mM EGTA, 0.2 mg/mL saponin, 1 mM ATP and 1% BSA, pH 7.5)[50]. The labeled neurons were then immediately fixed with 4 % PFA in PHEM buffer (60 mM PIPES, 25 mM HEPES, 10 mM EGTA, 2 mM $MgCl_2$, 0.12 M sucrose, pH 7.0) and labeled with phalloidin as described above.

Supplementary Material

Refer to Web version on PubMed Central for supplementary material.

Acknowledgement

This research is supported by grants from the National Institutes of Health to JQZ (GM083889 GM084363, and HD023315), JRB (NS40371), GC (NS054858), and HCH (EY014852 and GM60448).

References

1. Bredt DS, Nicoll RA. AMPA receptor trafficking at excitatory synapses. Neuron. 2003; 40:361–379. [PubMed: 14556714]

2. Collingridge GL, Isaac JT, Wang YT. Receptor trafficking and synaptic plasticity. Nat Rev Neurosci. 2004; 5:952–962. [PubMed: 15550950]
3. Malinow R, Malenka RC. AMPA receptor trafficking and synaptic plasticity. Annu Rev Neurosci. 2002; 25:103–126. [PubMed: 12052905]
4. Song I, Huganir RL. Regulation of AMPA receptors during synaptic plasticity. Trends Neurosci. 2002; 25:578–588. [PubMed: 12392933]
5. Yuste R, Bonhoeffer T. Morphological changes in dendritic spines associated with long-term synaptic plasticity. Annu Rev Neurosci. 2001; 24:1071–1089. [PubMed: 11520928]
6. Nimchinsky EA, Sabatini BL, Svoboda K. Structure and function of dendritic spines. Annu Rev Physiol. 2002; 64:313–353. [PubMed: 11826272]
7. Segal M. Dendritic spines and long-term plasticity. Nat Rev Neurosci. 2005; 6:277–284. [PubMed: 15803159]
8. Matsuzaki M, Honkura N, Ellis-Davies GC, Kasai H. Structural basis of long-term potentiation in single dendritic spines. Nature. 2004; 429:761–766. [PubMed: 15190253]
9. Park M, et al. Plasticity-induced growth of dendritic spines by exocytic trafficking from recycling endosomes. Neuron. 2006; 52:817–830. [PubMed: 17145503]
10. Tada T, Sheng M. Molecular mechanisms of dendritic spine morphogenesis. Curr Opin Neurobiol. 2006; 16:95–101. [PubMed: 16361095]
11. Cingolani LA, Goda Y. Actin in action: the interplay between the actin cytoskeleton and synaptic efficacy. Nat Rev Neurosci. 2008; 9:344–356. [PubMed: 18425089]
12. Hotulainen P, Hoogenraad CC. Actin in dendritic spines: connecting dynamics to function. J Cell Biol. 2010; 189:619–629. [PubMed: 20457765]
13. Bernstein BW, Bamburg JR. ADF/cofilin: a functional node in cell biology. Trends Cell Biol. 2010; 20:187–195. [PubMed: 20133134]
14. Van Troys M, et al. Ins and outs of ADF/cofilin activity and regulation. Eur J Cell Biol. 2008; 87:649–667. [PubMed: 18499298]
15. Rex CS, et al. Different Rho GTPase-dependent signaling pathways initiate sequential steps in the consolidation of long-term potentiation. J Cell Biol. 2009; 186:85–97. [PubMed: 19596849]
16. Zhou Q, Homma KJ, Poo MM. Shrinkage of dendritic spines associated with long-term depression of hippocampal synapses. Neuron. 2004; 44:749–757. [PubMed: 15572107]
17. Chen LY, Rex CS, Casale MS, Gall CM, Lynch G. Changes in synaptic morphology accompany actin signaling during LTP. J Neurosci. 2007; 27:5363–5372. [PubMed: 17507558]
18. Meng Y, et al. Abnormal spine morphology and enhanced LTP in LIMK-1 knockout mice. Neuron. 2002; 35:121–133. [PubMed: 12123613]
19. Sankaranarayanan S, De Angelis D, Rothman JE, Ryan TA. The use of pHluorins for optical measurements of presynaptic activity. Biophys J. 2000; 79:2199–2208. [PubMed: 11023924]
20. Lin DT, Huganir RL. PICK1 and phosphorylation of the glutamate receptor 2 (GluR2) AMPA receptor subunit regulates GluR2 recycling after NMDA receptor-induced internalization. J Neurosci. 2007; 27:13903–13908. [PubMed: 18077702]
21. Takumi Y, Ramirez-Leon V, Laake P, Rinvik E, Ottersen OP. Different modes of expression of AMPA and NMDA receptors in hippocampal synapses. Nat Neurosci. 1999; 2:618–624. [PubMed: 10409387]
22. Anikstejn L, Ben-Ari Y. Novel form of long-term potentiation produced by a K+ channel blocker in the hippocampus. Nature. 1991; 349:67–69. [PubMed: 1845914]
23. Ashby MC, Maier SR, Nishimune A, Henley JM. Lateral diffusion drives constitutive exchange of AMPA receptors at dendritic spines and is regulated by spine morphology. J Neurosci. 2006; 26:7046–7055. [PubMed: 16807334]
24. Allison DW, Gelfand VI, Spector I, Craig AM. Role of actin in anchoring postsynaptic receptors in cultured hippocampal neurons: differential attachment of NMDA versus AMPA receptors. J Neurosci. 1998; 18:2423–2436. [PubMed: 9502803]
25. Bubb MR, Senderowicz AM, Sausville EA, Duncan KL, Korn ED. Jasplakinolide, a cytotoxic natural product, induces actin polymerization and competitively inhibits the binding of phalloidin to F-actin. J Biol Chem. 1994; 269:14869–14871. [PubMed: 8195116]

26. Aizawa H, et al. Phosphorylation of cofilin by LIM-kinase is necessary for semaphorin 3A-induced growth cone collapse. Nat Neurosci. 2001; 4:367–373. [PubMed: 11276226]
27. Heredia L, et al. Phosphorylation of actin-depolymerizing factor/cofilin by LIM-kinase mediates amyloid beta-induced degeneration: a potential mechanism of neuronal dystrophy in Alzheimer's disease. J Neurosci. 2006; 26:6533–6542. [PubMed: 16775141]
28. Aunis D, Bader MF. The cytoskeleton as a barrier to exocytosis in secretory cells. J Exp Biol. 1988; 139:253–266. [PubMed: 3062121]
29. Eitzen G. Actin remodeling to facilitate membrane fusion. Biochimica et Biophysica Acta. 2003; 1641:175–181. [PubMed: 12914958]
30. Lanzetti L. Actin in membrane trafficking. Curr Opin Cell Biol. 2007; 19:453–458. [PubMed: 17616384]
31. Spector I, Shochet NR, Kashman Y, Groweiss A. Latrunculins: novel marine toxins that disrupt microfilament organization in cultured cells. Science. 1983; 219:493–495. [PubMed: 6681676]
32. Kim CH, Lisman JE. A role of actin filament in synaptic transmission and long-term potentiation. J Neurosci. 1999; 19:4314–4324. [PubMed: 10341235]
33. Hotulainen P, et al. Defining mechanisms of actin polymerization and depolymerization during dendritic spine morphogenesis. J Cell Biol. 2009; 185:323–339. [PubMed: 19380880]
34. Racz B, Weinberg RJ. Spatial organization of cofilin in dendritic spines. Neuroscience. 2006; 138:447–456. [PubMed: 16388910]
35. Makino H, Malinow R. AMPA receptor incorporation into synapses during LTP: the role of lateral movement and exocytosis. Neuron. 2009; 64:381–390. [PubMed: 19914186]
36. Heine M, et al. Surface mobility of postsynaptic AMPARs tunes synaptic transmission. Science. 2008; 320:201–205. [PubMed: 18403705]
37. Rust MB, et al. Learning, AMPA receptor mobility and synaptic plasticity depend on n-cofilin-mediated actin dynamics. Embo J. 2010; 29:1889–1902. [PubMed: 20407421]
38. Han L, et al. Direct stimulation of receptor-controlled phospholipase D1 by phosphocofilin. Embo J. 2007; 26:4189–4202. [PubMed: 17853892]
39. Fukazawa Y, et al. Hippocampal LTP is accompanied by enhanced F-actin content within the dendritic spine that is essential for late LTP maintenance in vivo. Neuron. 2003; 38:447–460. [PubMed: 12741991]
40. Okamoto K, Nagai T, Miyawaki A, Hayashi Y. Rapid and persistent modulation of actin dynamics regulates postsynaptic reorganization underlying bidirectional plasticity. Nat Neurosci. 2004; 7:1104–1112. [PubMed: 15361876]
41. Yuen EY, Liu W, Kafri T, van Praag H, Yan Z. Regulation of AMPA Receptor Channels and Synaptic Plasticity by Cofilin Phosphatase Slingshot in Cortical Neurons. J Physiol.
42. Onuma H, et al. A calcineurin inhibitor, FK506, blocks voltage-gated calcium channel-dependent LTP in the hippocampus. Neurosci Res. 1998; 30:313–319. [PubMed: 9678635]
43. Wang Z, et al. Myosin Vb mobilizes recycling endosomes and AMPA receptors for postsynaptic plasticity. Cell. 2008; 135:535–548. [PubMed: 18984164]
44. Schulz TW, et al. Actin/alpha-actinin-dependent transport of AMPA receptors in dendritic spines: role of the PDZ-LIM protein RIL. J Neurosci. 2004; 24:8584–8594. [PubMed: 15456832]
45. Lee CW, et al. Regulation of acetylcholine receptor clustering by ADF/cofilin-directed vesicular trafficking. Nat Neurosci. 2009; 12:848–856. [PubMed: 19483689]
46. Hoogenraad CC, Akhmanova A, Galjart N, De Zeeuw CI. LIMK1 and CLIP-115: linking cytoskeletal defects to Williams syndrome. Bioessays. 2004; 26:141–150. [PubMed: 14745832]
47. Campbell RE, et al. A monomeric red fluorescent protein. Proc Natl Acad Sci U S A. 2002; 99:7877–7882. [PubMed: 12060735]
48. Flynn KC, Pak CW, Shaw AE, Bradke F, Bamburg JR. Growth cone-like waves transport actin and promote axonogenesis and neurite branching. Dev Neurobiol. 2009; 69:761–779. [PubMed: 19513994]
49. Deng L, et al. Sequential postsynaptic maturation governs the temporal order of GABAergic and glutamatergic synaptogenesis in rat embryonic cultures. J Neurosci. 2007; 27:10860–10869. [PubMed: 17913919]

50. Schafer DA, et al. Visualization and molecular analysis of actin assembly in living cells. J Cell Biol. 1998; 143:1919–1930. [PubMed: 9864364]

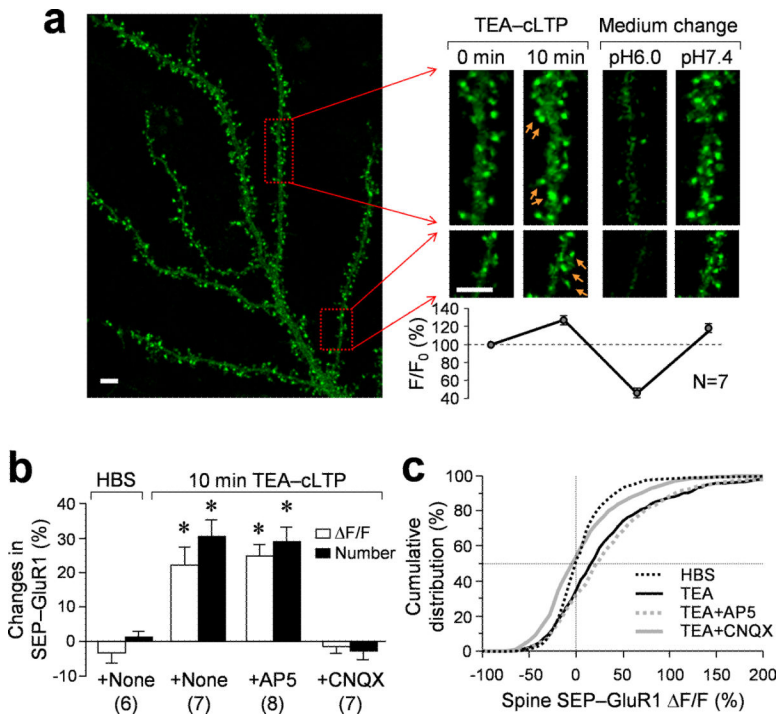

Figure 1.

Rapid addition of postsynaptic AMPA receptors to spine surface during chemical LTP induction by TEA. (**a**) Representative images of a DIV21 hippocampal neuron expressing SEP-GluR1 as revealed by live 3D confocal imaging. Dendritic regions enclosed by red boxes were shown in a higher magnification before (0 min) and 10 min after 25 mM TEA treatment for cLTP induction. Arrows indicate spines with new GluR1 addition. Application of a non-permeable acid buffer (pH 6.0) caused a marked loss of SEP-GluR1 fluorescence, which can be restored after changing back to a buffer of pH 7.4. The plot shows the quantification of fluorescent changes in correspondence to different treatments to the cells as depicted in the magnified panels. (**b**) Quantified data showing the changes in the integrated intensity of SEP-GluR1 fluorescence on all spines and the number of spines with bright SEP-GluR1 fluorescence after 10 min exposure to either Hepes-bufffered saline (HBS) or 25 mM TEA for cLTP induction without or with CNQX or AP5 treatment. Numbers in parentheses represent the number of cells examined for each condition. Asterisk: $p<0.01$ (Student's *t*-test). (**c**) Cumulative distribution curve of SEP-GluR1 fluorescence change on all individual spines showing significant receptor insertion after TEA treatment. CNQX blocks the insertion, whereas AP5 does not have a significant effect. Scale bar = 5 μm. Error bars in (a & b) represent standard error of the mean (s.e.m.).

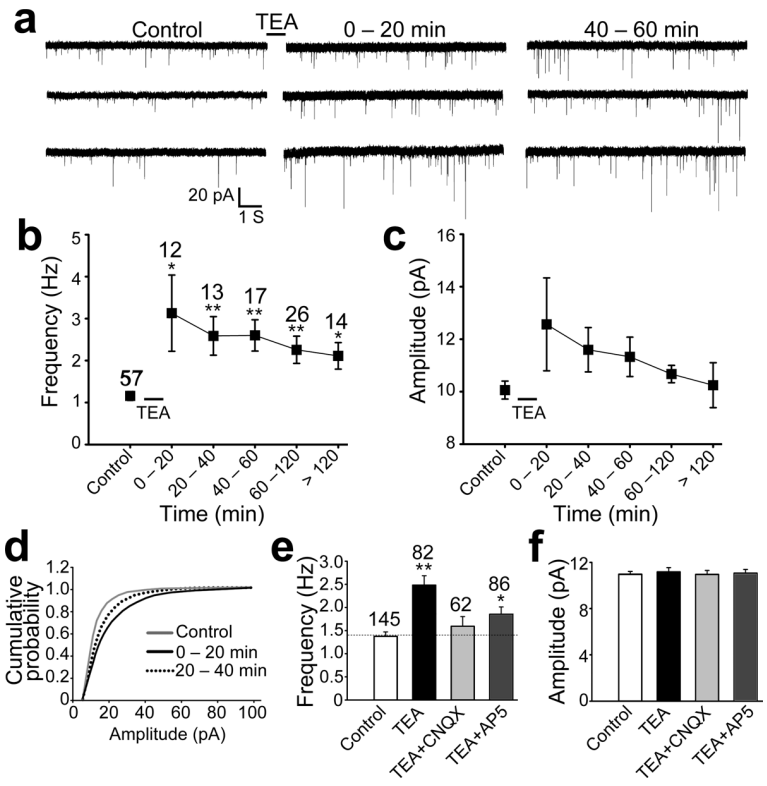

Figure 2.

Long-term potentiation of synaptic function induced by TEA treatment. (**a**) Representative traces showing mEPSCs before and after 10 min TEA stimulation. (**b**) Quantified data showing TEA-induced increase in the mEPSC frequency. Control mEPSC frequency = 1.2 ± 0.1Hz; After TEA treatment, the mEPSC frequency was: 0–20 min, 3.1 ± 0.9 Hz, $p<0.05$; 20–40 min, 2.6 ± 0.5 Hz, $p<0.01$; 40–60 min, 2.6 ± 0.4 Hz, $p<0.002$; 60–120 min, 2.3 ± 0.4 Hz, $p<0.004$; >120 min, 2.1 ± 0.3 Hz, $p<0.02$. Asterisks: $p<0.05$; double asterisks: $p<0.01$ (two-tailed Student's *t*-test comparing to the control). The numbers of cells examined in each group are shown above each data point. (**c**) Quantified data showing the changes of average mEPSC amplitude (median value) before and after TEA treatment. Control mEPSC amplitude = 10.1 ± 0.3 pA. After TEA treatment, the mEPSC amplitude was: 0–20 min, 12.6 ± 1.8 pA, $p>0.1$; 20–40 min, 11.6 ± 0.8 pA, $p>0.1$; 40–60 min, 11.3 ± 0.8 pA, $p>0.1$; 60–120 min, 10.7 ± 0.3 pA, $p>0.2$; >120 min, 10.2 ± 0.9 pA, $p>0.8$. (**d**) Cumulative distribution curve showing a significant potentiation of the mEPSC amplitude after TEA treatment ($p<0.0001$, Kolmogorov-Smirnov test). (**e**) Quantified data showing the effect of CNQX and AP5 on TEA-induced changes in the mEPSC frequency, which was determined from the entire recording over 2 hr after 10 min TEA stimulation. Single asterisk: $p<0.05$; double asterisks: $p<0.01$ (Student *t*-test). The numbers of cells examined in each group are shown above the bars. (**f**) The effects of CNQX and AP5 on TEA-induced changes of the mEPSC amplitude (averaged from all mEPSCs after TEA stimulation). No significant difference was observed ($p>0.5$, *t*-test). Error bars represent s.e.m.

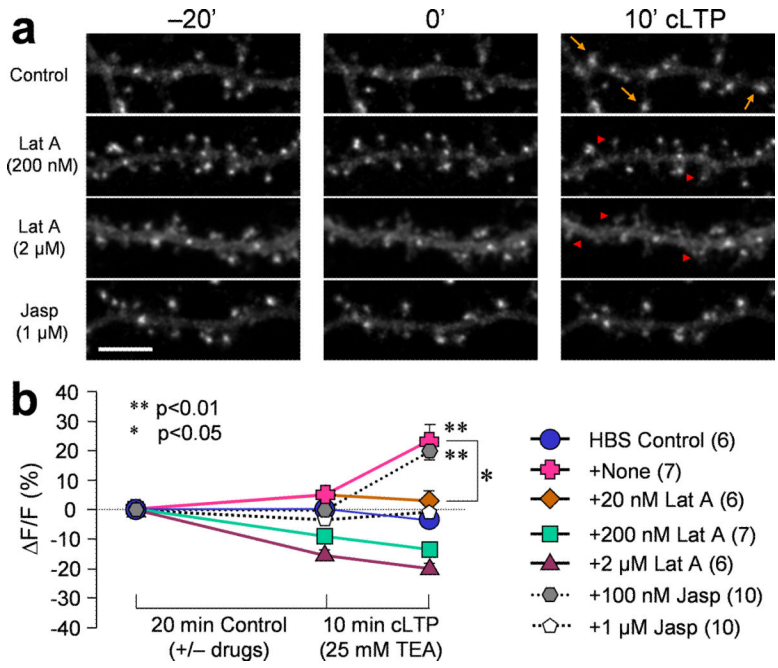

Figure 3.

Effects of actin drugs on TEA-induced AMPAR insertion. (**a**) Representative fluorescent images showing SEP-GluR1 fluorescence on dendritic regions before (−20') and after (0') 20 min of actin drug treatment, followed by 10 min cLTP induced by TEA. Arrows indicate spines with marked SEP-GluR1 addition. Arrowheads indicate spines with loss in SEP-GluR1 fluorescence. Scale bar = 10 μm. (**b**) Quantification showing the intergrated intensity of SEP-GluR1 fluorescence on all spines. Lat A: Latrunculin A; Jasp: Jasplakinolide. Error bars represent s.e.m. Numbers in parentheses represent the number of cells examined for each condition.

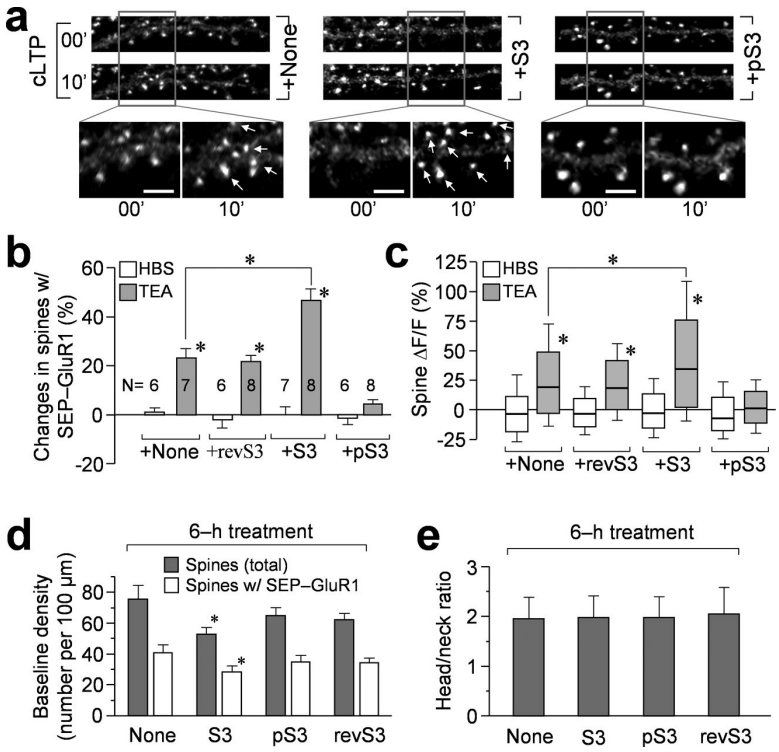

Figure 4.

Effects of S3 and pS3 peptides on TEA-induced GluR1 addition. (**a**) Representative images showing SEP-GluR1 fluorescence on dendritic regions before and after cLTP induction by 10 min TEA treatment. The neurons were treated with different peptides for 6 hr prior to cLTP treatment. Regions enclosed by the box are shown at a higher magnification. Arrows indicate sites of new SEP-GluR1 addition. Scale bar = 5 μm. (**b**) Quantification showing the changes in the number of bright SEP-GluR1 puncta after 10 min TEA or HBS treatment. Asterisks: $p<0.01$ comparing to the HBS group by Student's *t*-test. The TEA+S3 group is statistically different from the TEA group ($p<0.01$). Numbers indicate the number of cells examined in each group. (**c**) The box-whisker plot showing the changes of SEP-GluR1 fluorescence (ΔF/F) of all individual spines after 10 min TEA or HBS treatment. The bottom and top of the box represent the 25th and 75th percentile and the line near the middle of the box depicts the median (50%). The ends of the whiskers represent the 15th and 85th percentiles, respectively. Standalone asterisk: $p<0.01$ comparing to the HBS control (*t*-test). The asterisk for compared TEA and TEA+S3 groups: $p<0.01$ (*t*-test). (**d**) Quantification showing the baseline density of spine number and SEP-GluR1 puncta number before and after 6 hr peptide treatment. Asterisk: $p<0.05$ compared to the group without peptide treatment (Student's *t*-test). (**e**) Analysis of the spine head/neck ratio after 6 hr peptide treatment. Error bars in (b, d, e) represent s.e.m.

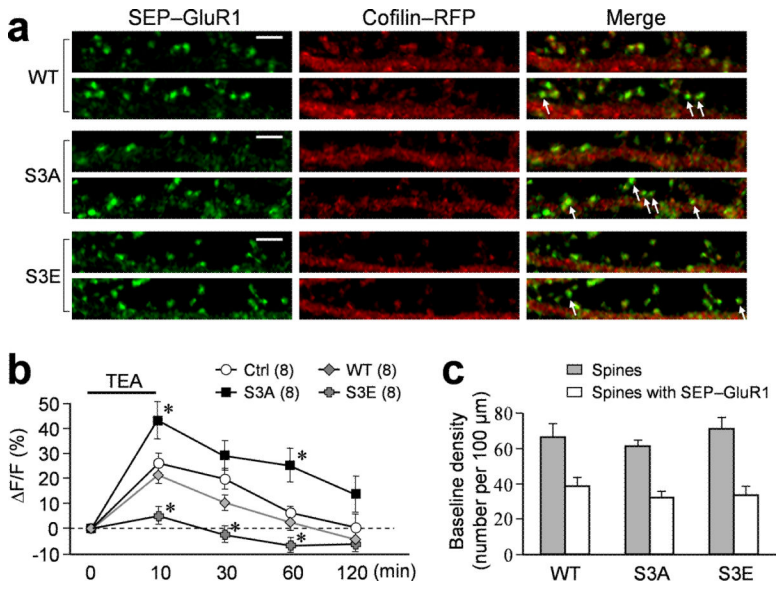

Figure 5.

Effects of different cofilin mutants on TEA-induced GluR1 addition. (**a**) Representative images of dendritic regions from neurons co-expressing SEP-GluR1 and different cofilin-RFP proteins before and after cLTP. Arrows indicate spines with substantial addition of new SEP-GluR1. Scale bar = 5 μm. Numbers in parentheses represent the number of cells examined for each condition. (**b**) Quantification of the integrated intensity of SEP-GluR1 fluorescence on all spines at different time points before and after TEA treatment. Numbers in parentheses indicate the number of cells examined. Asterisks: $p<0.05$ comparing to the same time point of the control group exposed to TEA only. (**c**) Quantified data showing the baseline density of spine number and bright SEP-GluR1 puncta. Error bars represent s.e.m.

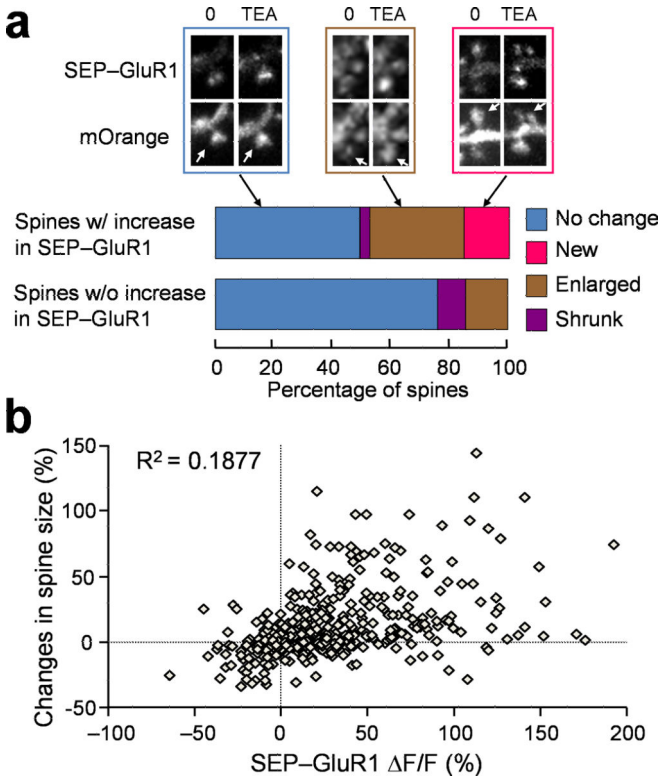

Figure 6.

Quantitative analyses of the spine size in relation to SEP-GluR1 insertion for neurons expressing both mOrange and SEP-GluR1. (**a**) Representative images display three types of changes in spines that exhibited SEP-GluR1 addition after TEA treatment: no change, increase in size, new spine. All the spines were analyzed and grouped into two: the ones exhibiting marked increase in SEP-GluR1 fluorescence and the one showing no change in SEP-GluR1 fluorescence. Quantification data show the percentage of each type of spine in two groups. Over 200 spines in total were analyzed for each condition. (**b**) Scatter plot showing the distribution of receptor insertion vs. size change of each individual spine.

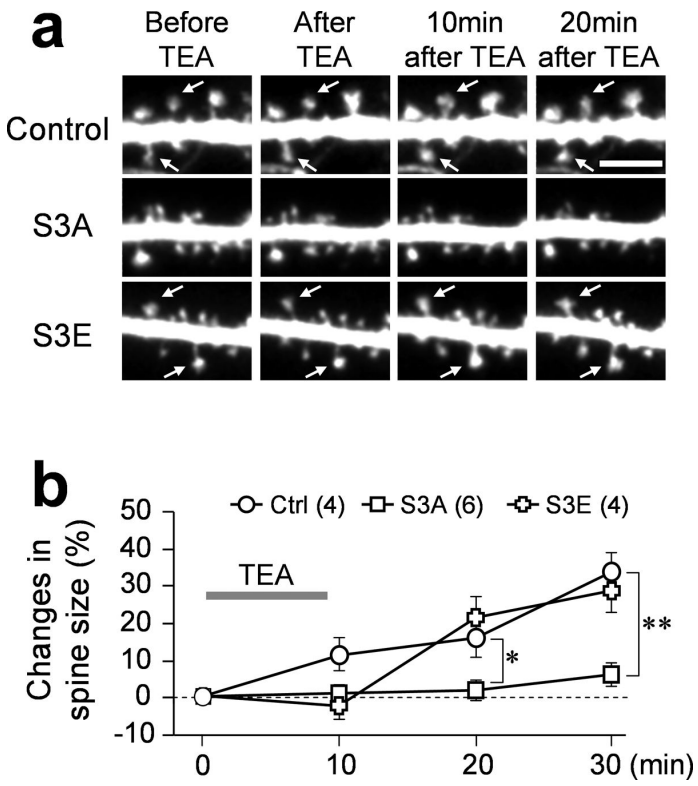

Figure 7.

Effects of different cofilin mutants on TEA-induced spine enlargement. (**a**) Representative images of dendritic regions from neurons expressing GFP only (Control) or with different RFP-cofilin mutants before and after cLTP. Arrows indicate spines exhibiting substantial increase of size after TEA treatment. Scale bar = 5 μm. (**b**) Quantification showing the change of spine size at different time points before and after TEA treatment. Over 200 spines in total were analyzed for each group. Asterisk: $p<0.05$, double asterisks: $p<0.01$, comparing to control group (ANOVA, Dunnett's test). Error bars represent s.e.m. Numbers in parentheses indicate the number of cells examined in each group.

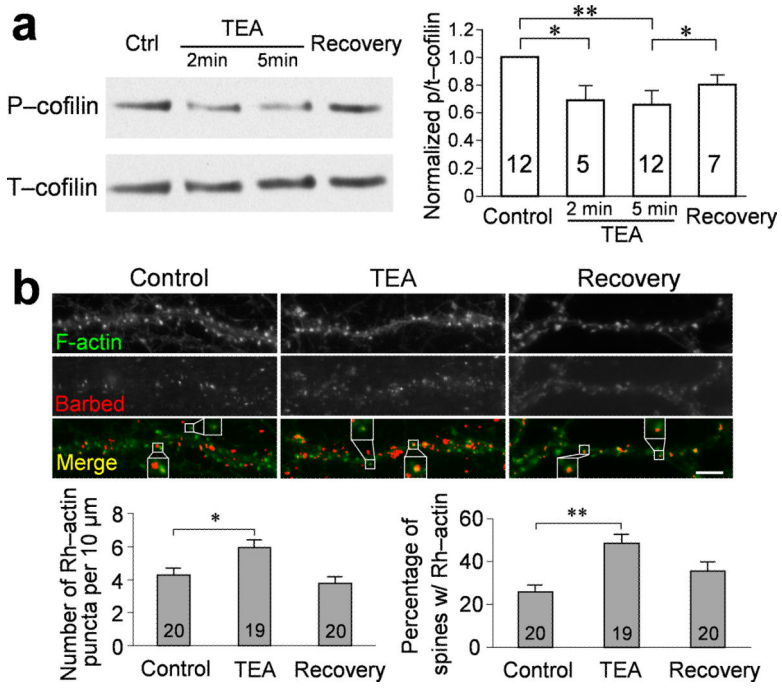

Figure 8.

Transient activation of cofilin and increase in actin barbed ends during cLTP induction by TEA. (**a**) A representative sample of a western blot of hippocampal culture extracts without TEA treatment (control), 2 min or 5 min after TEA treatment, and 30 min after TEA washout (recovery), using antibodies that recognize phospho-Ser3 cofilin. The film was then stripped and probed for the total cofilin level using a pan cofilin antibody. Quantification of the western blotting results is presented by the p/t-cofilin ratio. Numbers represent the rounds of experiments used to generate the average shown in the bar graph. Asterisks: $p<0.05$; double asterisks: $p<0.01$ (Mann-Whitney test). (**b**) Visualization of actin barbed ends and F-actin with and without cLTP induction by TEA. Representative images show the double staining of F-actin (green) and actin barbed ends (red) on dendritic segments without TEA treatment (control), immediately after 10 min TEA treatment (TEA), and 30 min after TEA washout (recovery). Spines enclosed by the boxes were shown in a higher magnification to exhibit the presence of barbed ends in spines. The barbed end signals were pseudocolored in red after applying an intensity threshold, and subsequently superimposed on the F-actin images to generate the color panels. Quantification in left panel shows the density of actin barbed ends on dendrites increased after cLTP. Quantification in right panel shows the percentage of spines containing actin barbed ends increased after cLTP. Numbers represent the number of cells examined in each group. Scale bar = 5 µm. Asterisk: $p<0.05$, double asterisks: $p<0.01$ when comparing to the control group (Student's *t*-test). Error bars represent s.e.m.